Correlation between structure, phonon spectra, thermal expansion, and thermomechanics of single-layer MoS_2

Liang Feng Huang,[1,2] Peng Lai Gong,[1] and Zhi Zeng[1,3,*]

[1]*Key Laboratory of Materials Physics, Institute of Solid State Physics, Chinese Academy of Sciences, Hefei 230031, China*

[2]*Department of Computational Materials Design, Max-Planck-Institut für Eisenforschung GmbH, Max-Planck-Str. 1, 40237 Düsseldorf, Germany*

[3]*University of Science and Technology of China, Hefei 230026, China*

(Received 4 June 2014; revised manuscript received 30 June 2014; published 15 July 2014)

Using first-principles simulation, the correlation between structure, phonon spectra, thermal expansion, and thermomechanics of single-layer MoS_2 is established. The laminar structure results in the low-dimension ZA mode with a parabolic dispersion and negative Grüneisen constants (γ), while the nonorthogonal covalent Mo–S bonds (or intralayer thickness) result in the interatom and interdirection vibrational hybridizations, which tend to increase γ. There is a negative-positive crossover in thermal expansion coefficient at 20 K, because of the competition between the modes with negative and positive γ. Although the phononic activation at finite temperatures has a stiffening effect on the bulk modulus, the dominant effect from thermal expansion softens the lattice upon heating. The intralayer thickness results in the similarity between the thermal expansions of SL and bulk MoS_2. Our numerical results explicitly support that the experimentally measured thermal shifts of the Raman modes are dominated by multiphonon scattering, but not thermal expansion.

DOI: 10.1103/PhysRevB.90.045409 PACS number(s): 63.20.dk, 63.22.−m, 65.40.Ba, 65.40.De

I. INTRODUCTION

The structural exploration and property investigation of two-dimensional materials in recent work [1–8] are excited by the advent of graphene [9], a two-dimensional carbon allotrope with superior electronic, mechanical, chemical, optical, and biological properties [10–12]. Apart from graphene, MoS_2 is another promising two-dimensional material, whose bulk counterpart has been used as the dry lubrication and catalysis in industry, and also has shown potential photovoltaic and photocatalytic properties [4]. From bulk to few layer (FL) and single layer (SL), the band gap of MoS_2 has an indirect-direct transition, which considerably increases its light absorption [13–15], and implies its promising applications in optical devices. Due to the finite band gap (1.9 eV), high on/off ratios (10^3–10^8) also have been realized in SL MoS_2 transistors [16–18].

The lattice constant and stiffness of MoS_2, as well as their temperature dependence, are very important for the design of related electronic and optical devices, because any accumulated internal stress/strain will degrade the performance or even damage the devices when used under varying temperatures. It also has been found that the band gaps and vibrational frequencies of many semiconducting transition-metal dichalcogenides (including MoS_2) have a sensitive dependence on the lattice constant [19–24]. The vibrational modes and frequencies can give out essential elemental information about the materials, and are also important for the understanding of many experimental characterizations. Several groups have simulated the phonon dispersions and thermodynamic properties of MoS_2, and various experimental Raman measurements also have been well understood [20,22,25–28]. However, the roles of Mo and S atoms in the whole phonon dispersions are still not clear, which are important to understand the interatom interaction/cooperation in vibrations. And a systematic correlation between structure, phonons, anharmonicity, thermodynamic functions, thermal expansion, and thermomechanics still has not been established. Currently available experimental measurements on the thermal expansion and frequency thermal shift also require further theoretical explanation. In addition, there is a disagreement on the Grüneissen constant of the flexural ZA mode in SL MoS_2 between two theoretical groups (positive [22] versus negative [27]). The convergence of the flexural modes is hard to be obtained in simulation; thus a stringent calculation and a clear physics are needed to settle this disagreement.

In this work, the phonon dispersions, thermal expansion, and temperature-dependent bulk modulus of SL MoS_2 are calculated using first-principles simulation. The correlation between structure (a planar sheet with a thickness), phonon dispersions, interatom and interdirection vibrational hybridizations, Grüneisen constants, thermal expansion, and thermomechanics is established. Our results have provided clear physical mechanisms underlying the experimental measurements on the thermal expansion and thermal redshift of Raman modes.

II. COMPUTATIONAL AND THEORETICAL METHODS

The structure, electronic structure, and energy are calculated using density functional theory (DFT), and the phonons are calculated using density functional perturbation theory (DFPT) [29]. The DFT and DFPT calculations are carried out using the Quantum ESPRESSO code [30], which uses the planewave-pseudopotential method. The ultrasoft [31] PBE [32] pseudopotentials are used to describe the electronic exchange and correlation. The cutoff energies for the wave function and charge density are 50 and 500 Ry, respectively. The k-point grid for the electronic-state integration is $12 \times 12 \times 1$. An interlayer distance of 15 Å in the periodic cell is large enough to exclude the interlayer interaction. The k-point

*zzeng@theory.issp.ac.cn

grid for the calculation of dynamical matrices is $12 \times 12 \times 1$, and that for the calculation of thermodynamic properties is $50 \times 50 \times 1$. A k-point grid of $200 \times 200 \times 1$ is used to calculate the phonon density of states (PhDOS), as well as the projected PhDOSs for the in-plane (XY) and out-plane (Z) vibrations of the Mo and S atoms. To precisely calculate the frequencies of the flexural ZA modes near the Brillouin-zone center, stringent convergence thresholds (10^{-12} and 10^{-8} Ry) for the total electronic energy and the perturbation of the self-consistent potential ($\Delta V_{\rm scf}$) are required, which are also necessary for pristine and functionalized graphene [33]. It should be noted that the Quantum ESPRESSO code uses the square of the differential $\Delta V_{\rm scf}$ ($=10^{-16}$ here) as the convergence threshold during iterative phonon calculations.

The temperature dependences of the lattice constant and bulk modulus are simulated using the quasiharmonic approximation (QHA), which takes the first-order anharmonicity into account [34]. QHA has been used to calculate the thermal expansions of diamond, graphite, and graphene [27,35], and theory-experiment agreements have been reached for the former two within a large temperature range (0–3000 K). In experiment, the thermal expansion of graphene is indirectly derived from the thermal shift of Raman-active modes. Although an experimental consensus on graphene still has not been achieved [36–38], part of the experimental results [38] agree well with the DFT-QHA results [27,33,35]. SL MoS_2 has a thickness of ~3.1 Å, which makes it more like graphite [35] or functionalized graphene [33] than pristine graphene; thus QHA is expected to be reliable here. The temperature-dependent lattice constant can be derived from the free energy in QHA [33]

$$a(T) = \left(\frac{dE^e(a)}{da}\right)^{-1} \frac{1}{N_k} \sum_{k,\sigma} U_{k,\sigma}\gamma_{k,\sigma}, \tag{1}$$

where N_k is the number of k points; k and σ are the indices of the wave vector and branch of a phonon mode; E^e, $U_{k,\sigma}$, and $\gamma_{k,\sigma}$ are the electronic energy, and the internal energy and Grüneisen constant of the (k,σ) vibrational mode, respectively. γ is defined as

$$\gamma = -\frac{a}{\omega}\frac{d\omega}{da}, \tag{2}$$

and the frequency shift caused by thermal expansion is also considered

$$\omega(a + \Delta a) = \left(1 - \gamma\frac{\Delta a}{a}\right)\omega(a). \tag{3}$$

From Eq. (1), the thermal expansion coefficient can be derived as

$$\alpha(T) = \frac{1}{a(T)}\frac{da(T)}{dT} = \frac{1}{s_1 + s_2 + s_3}\frac{1}{N_k}\sum_{k,\sigma} C^V_{k,\sigma}\gamma_{k,\sigma}, \tag{4}$$

where $C^V_{k,\sigma}$ is the isovolume heat capacity of the (k,σ) mode, and

$$s_1 = a^2\frac{d^2E^e(a)}{da^2}, \quad s_2 = a\frac{dE^e(a)}{da},$$
$$s_3 = \frac{1}{N_k}\sum_{k,\sigma}\left[U_{k,\sigma} - TC^V_{k,\sigma}\right]\gamma^2_{k,\sigma}. \tag{5}$$

The lattice constant at the lowest temperature is determined by iteratively solving Eqs. (1)–(3), and then $a(T)$ is calculated one shot from low to high temperatures using

$$a(T + \Delta T) = [1 + \alpha(T)\Delta T]a(T). \tag{6}$$

The two-dimensional bulk modulus ($B_{\rm 2D} = A\frac{\partial^2 F_{\rm tot}}{\partial A^2}$, where A is the area) is used to describe the stiffness of SL MoS_2, which is derived to be

$$B_{\rm 2D}(T) = \frac{1}{2\sqrt{3}a^2}[s_1 - s_2 + s_3 + s_4], \tag{7}$$

where

$$s_4 = \frac{2}{N_k}\sum_{k,\sigma} U_{k,\sigma}\gamma_{k,\sigma}. \tag{8}$$

In a planar two-dimensional lattice, the parabolically dispersing flexural ZA mode results in a nonzero PhDOS at $\omega = 0$ and then the divergent thermal excitation at finite temperature [33]. This is the reason why there is no low-dimensional lattice having strictly crystalline order at finite temperature [39]. The existence of the suspended two-dimensional lattices (e.g., SL graphene and MoS_2) is ascribed to the stabilizing effect from the intrinsic ripples [40–42]. Intrinsic ripples of 60–100 Å also have been observed in suspended SL MoS_2 [43], which will destroy the long-wavelength phonons. In this work, the phonons with wavelength larger than 80 Å are excluded in the thermodynamic simulations.

III. RESULTS AND DISCUSSION

SL MoS_2 has a hexagonal lattice with three atoms per unit cell, and the Mo layer is sandwiched between two S layers. The calculated structure of SL MoS_2 is shown in Fig. 1(a), where the lattice constant, thickness, Mo-S bond length, ∠MoSMo, and ∠SMoS are 3.193, 3.134, 2.415 Å, 82.8°, and 80.5°, respectively, which are consistent with other reported results [8,21,25,27]. The lattice constant is overestimated by 1% when compared with experimental measurement (3.16 Å) [25], which is well known due to the generalized gradient approximation used in the PBE potential [32]. However, this overestimation in equilibrium constant will not influence the response of the lattice to heat. The differential electron density (ΔQ) and its projection onto the out-plane (z) direction (ΔQ_z) can be used to understand the bond character of MoS_2, which are shown in Fig. 1(b). It can be seen that the electrons flow from both Mo and S atoms into the Mo–S bonds, which indicates the high covalency of these bonds. The amount of depleting electrons on the S atoms is much less than that on the Mo atom, and the bond electrons are closer to the S atoms, both of which are due to the higher electronegativity of S than that of Mo. It has been found that MoS_2 is slightly polar and the LO-TO splitting is very small ($\lesssim$2.8 $\rm cm^{-1}$) [26,44], even comparable with or smaller than the mode width (2–5 $\rm cm^{-1}$) measured in experiments. This negligible polarity is due to both the symmetrical sandwich structure and high covalency of the Mo–S bonds. These nonorthogonal [Fig. 1(a)] and highly covalent [Fig. 1(b)] Mo–S bonds will effectively result in the hybridization between the in-plane (XY) and out-plane (Z) vibrations, and then play an important role in the thermodynamic properties of MoS_2.

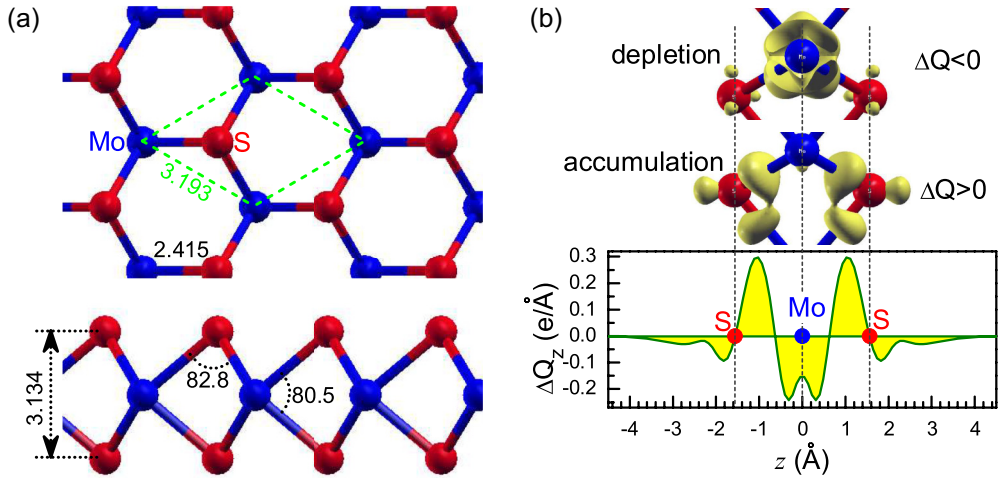

FIG. 1. (Color online) (a) Top and side views of SL MoS_2, where the lattice constant, bond length, thickness (in Å), and the Mo-S-Mo and S-Mo-S angles (in degrees) are labeled. (b) The differential electron density (ΔQ) (isovalues: $\pm 0.0675\ e/AA^3$) in real space and its z-direction projection (ΔQ_z).

The phonon dispersions and PhDOS of SL MoS_2 are shown in Fig. 2(a), where the phonon branches are sorted according to the continuity of their eigenvectors

$$\left|\sum_i \mathbf{e}^*_{k,\sigma_1}(i)\cdot\mathbf{e}_{k+\Delta,\sigma_2}(i)\right| = \left|\delta_{\sigma_1,\sigma_2} - O(\Delta)\right|, \qquad (9)$$

where $\mathbf{e}_{k,\sigma}(i)$ is the displacement of the atom i in the eigenvector of (k,σ) vibrational mode, and Δ is a small wave vector. The $k\cdot p$ theory for phonons is implicitly used in this branch sorting. The experimentally measured frequencies of the optical modes at Γ point [19,45–50] agree with our theoretical results, except for a small systematic underestimation of 5–10 cm^{-1} in the latter, which is due to the overestimation of the lattice constant by the PBE potential. According to previous works on pristine and functionalized graphene [35,51], such small downshift in frequency will not have any observable effect on the temperature effects. The phonon bands with their widths weighted by the contribution of a specified atom and direction are called *fat bands*. The fat bands for the Mo(XY), Mo(Z), S(XY), and S(Z) vibrations are shown in Figs. 2(b) and 2(c), together with the corresponding projected PhDOSs. Although the LA and TA modes have normal linear dispersions near the Γ point, the flexural ZA mode has a parabolic dispersion and a finite PhDOS at $\omega = 0$ [Fig. 2(a)], which is an ubiquitous phenomenon in two-dimensional systems, e.g., pristine and functionalized graphene [33,35]. These flexural modes are unstable at finite temperatures due to their divergent thermodynamic functions, which is the reason why there is no long-range crystalline order in low-dimensional systems [39], and intrinsic ripples are inevitably observed in two-dimensional systems, e.g., graphene [40–42] and SL MoS_2 [43]. The ZA mode consists of the Mo(Z) and S(Z) vibrations at the Γ point, while the contribution from the S(XY) vibration becomes larger when getting away from the Γ point [Figs. 2(b) and 2(c)]. This XY-Z hybridization is caused by the nonorthogonality of the covalent Mo–S bonds (Fig. 1), which is similar in functionalized graphene [51], and is also ubiquitous in other vibrational modes of MoS_2. It can be seen from the fat bands and projected PhDOSs of Mo [Fig. 2(b)] that there is no hybridization between the Mo(XY) and Mo(Z) vibrations in all phonon branches, because the Mo layer is symmetrically sandwiched by two S layers, which makes the XY and Z vibrations of the Mo layer distinctive from each other. Therefore, the Mo(XY) or Mo(Z) vibration only hybridizes with the S(XY) and S(Z) vibrations, while the S(XY) and S(Z) vibrations can hybridize with each other. The highest two branches [ZO^s and ZO^{as}, Fig. 2(a)] mainly consist of the S(Z) vibration [Figs. 2(b) and 2(c)], and the two S layers have symmetric and antisymmetric displacements in them, respectively. The observable Mo(Z) vibration in the ZO^s branch [Fig. 2(b)] is required by the mass-center invariance, and there is also observable hybridization coming from the S(XY) vibration in the ZO^s branch near the Brillouin-zone boundary [Fig. 2(c)]. The ZO^s branch also has a parabolic dispersion and constant PhDOS near the Γ point. Other optical branches below the ZO^s and ZO^{as} ones mainly consist of the S(XY) vibration, and some hybridizations from the S(Z) and Mo(XY) vibrations are also observable [Figs. 2(b) and 2(c)].

The Grüneisen constants (γ) of the phonon branches are shown in Fig. 2(d). The most prominent phenomenon is the large negativity of γ(ZA) near the Γ point, which is consistent with Sevik's result [27]. This kind of negativity for the flexural modes has been found in various two-dimensional systems [27,33,35,51] or open-shell three-dimensional semiconductors [52], because of the membrane effect [35] or the guitar-string effect [52] present in the vibrational modes with low-dimensional character. However, Cai [22] has obtained an unphysically large positive value for γ(ZA) (=320), and γ(LA) and γ(TA) are also abnormally large (=55 and 120). This is probably caused by the poor frequency convergence used there, which is also implied by the unphysical wiggles in the γ of some optical branches in Cai's result [22]. In planar graphene, the γs of the ZA and ZO branches are fully negative [35,51]. While in SL MoS_2, γ(ZO) is positive, and γ(ZA) is only negative near the Γ point, which is similar in functionalized graphene [33,51]. This negative-positive conversion is due to the hybridization between the Z and XY

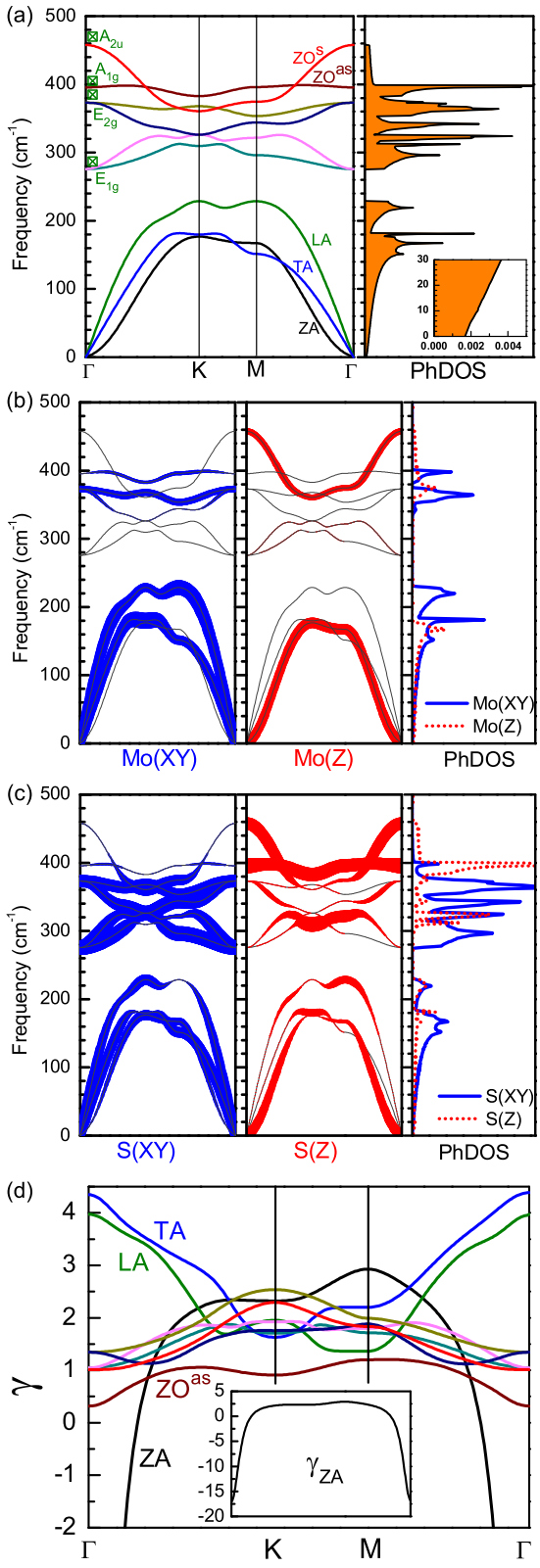

FIG. 2. (Color online) (a) Phonon dispersions and PhDOS, (b), (c) fat bands and projected PhDOSs, and (d) Grüneisen constants of SL MoS_2. In (a), the experimental frequencies of the optical modes (A_{2u}, A_{1g}, E_{2g}, E_{1g}) at the Γ point [19,45–50] are shown in the left panel, and the detailed PhDOS at low frequencies are shown in the inset of the right panel. In (d), the dispersion of γ(ZA) is fully shown in the inset.

vibrations, which is caused by the nonorthogonal covalent bonds in MoS_2 (and functionalized graphene). This also can be viewed as a thickness effect [33], which counteracts the membrane effect [35] in low-dimensional systems. When leaving from the Γ point, the contribution of the S(XY) vibration to the ZA mode becomes larger and larger [Fig. 2(c)], which makes the flexural ZA mode more and more like a normal mode with positive γ. γ always tends to increase with the contribution of the XY vibration, because the change in the lateral dimension will have more normal anharmonic effect on the XY than Z vibrations. The TA (LA) mode has its largest and lowest γ at the Γ and K (M) points [Fig. 2(d)], where the contributions of the S(Z) vibration are the smallest and largest [Fig. 2(c)], respectively. The same trend is also observable in all optical modes when comparing their γs [Fig. 2(d)] and fat bands [Fig. 2(c)]. The effect of XY-Z hybridization on the anharmonicity will play an important role in various thermodynamic properties of SL MoS_2, which will be discussed in the following.

The temperature dependences of the lattice constant (a), thermal-expansion coefficient (α), isovolume heat capacity (C_V), and two-dimensional bulk modulus (B_{2D}) are shown in Fig. 3. The melting point of MoS_2 is 1458 K, only below which the calculated properties are meaningful. The equilibrium lattice constant from DFT calculation is 3.193 Å, and the zero-point vibration expands the lattice by 0.15% at 0 K, which is smaller than those in diamond (0.4%), h-BN (0.3%), graphene (0.3%), and functionalized graphene (0.4%) [27,33,35,51]. The small zero-point expansion in SL MoS_2 is due to its large mass, which results in lower frequencies, smaller zero-point energy, and then smaller $a(0)$ [Eq. (1)]. In Fig. 3(a), the simulated $\frac{a(T)-a(0)}{a(0)}$ for SL MoS_2 is compared with available experimental results for bulk MoS_2 [53,54], where the highly nonlinear variation of the latter above 800 K is caused by oxidation [54]. It is interesting that the thermal expansions of SL and bulk MoS_2 are quite close to each other, though the former is a little smaller. However, the situation is totally different for graphene and graphite [35]. Graphite has a much larger thermal expansion than graphene, because the interlayer interaction in graphite considerably increases the γ of the ZA and ZO modes, which are fully negative in graphene and responsible for its thermal contraction [35]. This also can be viewed as a thickness effect. However, in SL MoS_2, the nonorthogonal Mo–S bonds (i.e., intralayer thickness) and the resulted XY-Z hybridization already have stiffened the ZO branch and most of the ZA branch, leading to the positive γ [Fig. 2(d)]. Thus there is little space for the interlayer stacking in bulk MoS_2 to influence the anharmonicity of those modes and then the lateral thermal expansion.

Considering the scattering data and the presence of oxidation in those early experiments [53,54], more accurate measurements on MoS_2 (SL, FL, and bulk) are still necessary. Understanding the redshift of Raman modes upon heating also requires the information about thermal expansion [45], the precision of which is expected to be influential on the conclusion. The thermal shifts of the Raman modes (E_{2g} and A_{1g}) have been measured by many experimental groups [45–48,56], and both thermal expansion and multiphonon scattering are expected to be contributive. By fitting experimental results using a simplified model, Najmaei [45] proposed that only

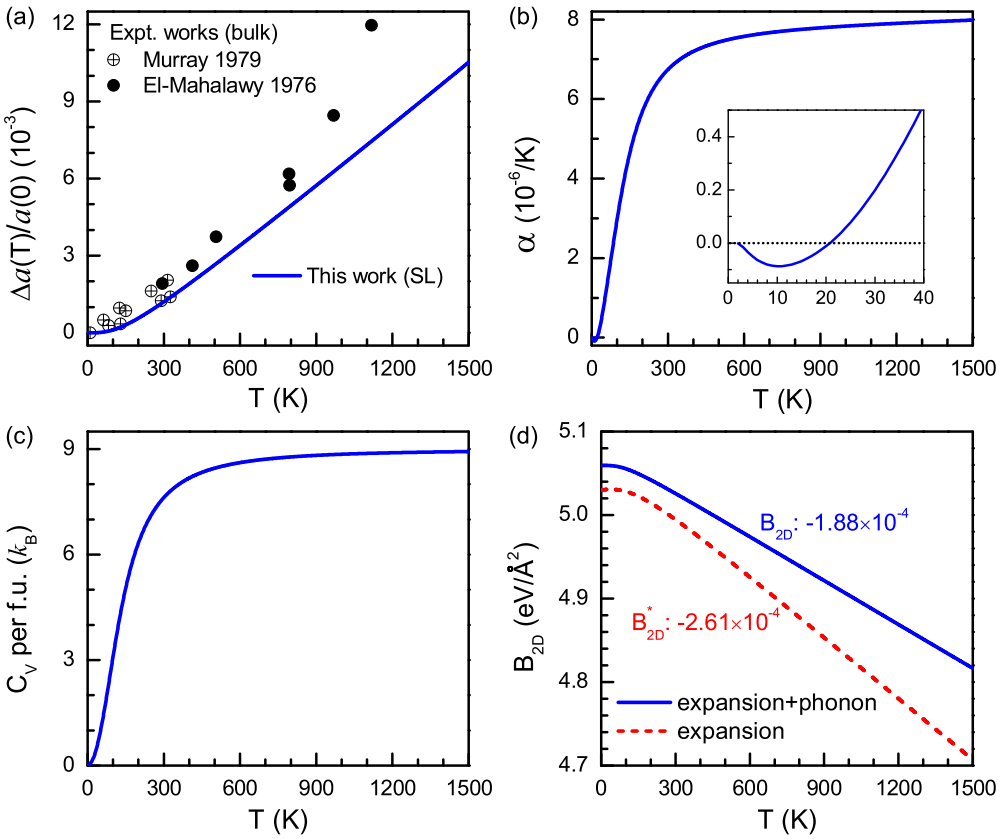

FIG. 3. (Color online) Temperature dependence of the (a) lattice constant, (b) thermal expansion coefficient, (c) isovolume heat capacity, and (d) two-dimensional bulk modulus of SL MoS_2. In (a), the available experimental measurements on bulk MoS_2 [53,54] are shown. In (b), the detailed variation of α at low temperature is shown in the inset. In (d), the bulk modulus with the phononic contribution excluded (B^*_{2D}) is shown, and the linear slopes of the curves are indicated.

multiphonon scattering contributes to the redshift of the E_{2g} mode upon heating, while in the redshift of the A_{1g} mode, the contribution of thermal expansion is even larger than that of multiphonon scattering. However, by combining experimental measurement and molecular-dynamics simulation, Lanzillo [47] proposed that only multiphonon scattering is sufficient to understand the redshifts of both E_{2g} and A_{1g} modes. We are intending to provide numerical calculation on the expansion-caused redshift (χ_{TE}) by using

$$\chi_{TE} = \frac{\partial\omega}{\partial a}\frac{da}{dT} = -\gamma\alpha\omega. \tag{10}$$

The calculated χ_{TE}s of the A_{2u}, A_{1g}, E_{2g}, and E_{2g} modes are listed in Table I, where the experimental thermal-shift rates of the A_{1g} and E_{2g} modes in suspended/supported SL, FL, and bulk MoS_2 [45–48,55] are also summarized. It is found that the calculated χ_{TE}s of the A_{1g} and E_{2g} modes are less than the experimental shift rates by one order of magnitude, even less than the variation between different experiments. This indicates that the redshift of any Raman modes in MoS_2 upon heating is dominated by the multiphonon scattering, which is consistent with Lanzillo's [47] conclusion.

When increasing temperature, the low-lying ZA modes with negative γ [Figs. 2(a) and 2(d)] will be activated first; thus SL MoS_2 has a thermal contraction (negative α) below 20 K [Fig. 3(b)]. However, at higher temperatures, the lattice converts into thermal expansion [positive α, Fig. 3(b)]. One fully activated phonon branch will contribute 1.0 k_B to C_V per formula unit, and it can be seen from Fig. 3(c) that most (86%) of the phonon branches already have been activated at 300 K. This easy activation of the vibrational modes is due to their low frequencies in heavy MoS_2, and the activation of the positive-γ modes is responsible for the thermal expansion of SL MoS_2 above 20 K. α increases quickly from 0 to 300 K due to the

TABLE I. Calculated expansion-caused shift rates (χ_{TE}, in cm^{-1}/K) of the A_{2u}, A_{1g}, E_{2g}, and E_{2g} modes in SL MoS_2, and the experimental thermal-shift rates of the A_{1g} and E_{2g} modes in suspended/supported SL, FL, and bulk MoS_2. The modes with Raman and infrared activity are labeled with "R" and "I," respectively.

	A_{2u} (I)	A_{1g} (R)	E_{2g} (I+R)	E_{2g} (R)
This work (χ_{TE})	**−0.0031**	**−0.0010**	**−0.0033**	**−0.0019**
Suspended SL [48]		−0.0130	−0.0110	
Supported SL [48]		−0.0130	−0.0170	
Supported SL [45]		−0.0143	−0.0179	
Supported SL [47]		−0.0160	−0.0130	
Suspended FL [55]		−0.0120	−0.0130	
Supported FL [46]		−0.0123	−0.0132	
Bulk [56]		−0.0123	−0.0147	

easy phononic activation, and then asymptotically approaches 8.0×10^{-6} K^{-1} at high temperatures, which explains the reason why a high degree of linearity already has been achieved in the $a(T)$ curve below 300 K [Fig. 3(a)]. The temperature dependence of the two-dimensional bulk modulus (B_{2D}) of SL MoS_2 is shown in Fig. 3(d), which consists of the contributions from both thermal expansion and phononic activation [Eq. (7)]. The $B_{2D}(T)$ curve enters into a highly linear variation above 150 K, and the linear slope is -1.88×10^{-4} eV Å^{-2} K^{-1}. To understand the roles of thermal expansion and phononic activation in $B_{2D}(T)$, the bulk modulus without phonon contribution (B^*_{2D}) is also calculated [Fig. 3(d)], namely, the s_3 and s_4 parameters are excluded in Eq. (7). This is the so-called *quasistatic approximation* proposed by Wang [57], which only considers the effect of thermal expansion in thermomechanics. At low temperatures (<100 K), B^*_{2D} is lower than B_{2D} by 0.6%, which is due to the stiffening effect of the zero-point vibrations in the latter. The $B^*_{2D}(T)$ curve also has a highly linear variation above 150 K, and the linear slope is -2.61×10^{-4} eV Å^{-2} K^{-1}, which is smaller than that of the $B_{2D}(T)$ curve. This indicates that the softening effect from the thermal expansion is partially canceled by the stiffening effect from the phonon activation in $B_{2D}(T)$. The frequency lowering caused by thermal expansion results in the increased activation of the phonons with positive γs, which then tends to increase B_{2D} [Eqs. (7) and (8)]. This phononic stiffening effect is different from the phononic softening effect in graphene [33], where the frequency heightening caused by thermal contraction tends to decrease B_{2D}. In pristine and functionalized graphene [33,51], B_{2D} has an increase within some temperature window due to the effect from the thermal contraction. However, the B_{2D} of SL MoS_2 monotonically decreases with increasing temperature, because the weak thermal contraction at low temperature (<20 K) cannot result in any observable increase in B_{2D}.

IV. CONCLUSION

The correlation between structure, phonon spectra, thermal expansion, and thermomechanics of single-layer MoS_2 has been investigated using first-principles simulation. The existence of the flexural ZA mode with a parabolic dispersion and negative Grüneisen constant (γ) is due to the low-dimensional structure. However, the nonorthogonal covalent Mo–S bonds (or intralayer thickness) result in the interatom and XY-Z vibrational hybridizations, and then tend to increase γ. There is a negative-positive crossover in the γ of ZA branch, which is also due to the phononic hybridization. A negative-positive crossover also exists in thermal expansion coefficient at 20 K, because of the competition between the modes with negative and positive γ. The calculated thermal expansion of single-layer MoS_2 is quite close to the experimental measurements on bulk MoS_2, because the chemical-bond nonorthogonality in MoS_2 layer has similar effect on γ and thermodynamic properties as the interlayer interaction in bulk MoS_2. Upon heating, the redshifts of the Raman modes caused by thermal expansion are smaller than experimental measurements by one order of magnitude, which indicates the dominant role of multiphonon scattering in those Raman shifts, and settles a disagreement on the importance of thermal expansion. Although both the phononic activation and low-temperature thermal contraction have a stiffening effect on the bulk modulus of single-layer MoS_2, the dominant effect from the positive thermal expansion consistently softens the lattice upon heating. The phonon spectra, Grüneisen constants, thermal expansion, and thermomechanics of SL MoS_2 are closely compared with those of pristine and functionalized graphene, and the concluded physical mechanisms should be helpful for further theoretical and experimental studies on other two-dimensional systems.

ACKNOWLEDGMENTS

The authors wish to thank D. Y. Liu for his supercomputer-technical support. This work is supported by the National Science Foundation of China under Grants No. 11204305 and No. U1230202(NSAF), the special Funds for Major State Basic Research Project of China (973) under Grant No. 2012CB933702, and Heifei Center for Physical Science and Technology under Grant No. 2012FXZY004. The calculations were performed in Center for Computational Science of CASHIPS and on the ScGrid of Supercomputing Center, Computer Network Information Center of CAS.

[1] K. S. Novoselov, D. Jiang, F. Schedin, T. J. Booth, V. V. Khotkevich, S. V. Morozov, and A. K. Geim, Proc. Natl. Acad. Sci. USA **102**, 10451 (2005).
[2] J. N. Coleman, M. Lotya, A. ONeill, S. D. Bergin, P. J. King, U. Khan, K. Young, A. Gaucher, S. De, R. J. Smith *et al.*, Science **331**, 568 (2011).
[3] C. N. R. Rao, H. S. S. Ramakrishna, and U. Maitra, Ang. Chem. Int. Ed. **52**, 13162 (2013).
[4] M. Xu, T. Liang, M. Shi, and H. Chen, Chem. Rev. **113**, 3766 (2013).
[5] S. Lebégue and O. Eriksson, Phys. Rev. B **79**, 115409 (2009).
[6] C. Ataca, H. Şahin, and S. Ciraci, J. Phys. Chem. C **116**, 8983 (2012).
[7] S. Lebégue, T. Björkman, M. Klintenberg, R. M. Nieminen, and O. Eriksson, Phys. Rev. X **3**, 031002 (2013).
[8] Y. Ding, Y. Wang, J. Ni, L. Shi, S. Shi, and W. Tang, Physica B **406**, 2254 (2011).
[9] K. S. Novoselov and A. K. Geim, Science **306**, 666 (2004).
[10] A. K. Geim and K. S. Novoselov, Nat. Mater. **6**, 183 (2007).
[11] V. Singh, D. Joung, L. Zhai, S. Das, S. I. Khondaker, and S. Seal, Prog. Mater. Sci. **56**, 1178 (2011).
[12] A. H. C. Neto, F. Guinea, N. M. R. Peres, K. S. Novoselov, and A. K. Geim, Rev. Mod. Phys. **81**, 109 (2009).
[13] K. F. Mak, C. Lee, J. Hone, J. Shan, and T. F. Heinz, Phys. Rev. Lett. **105**, 136805 (2010).
[14] A. Splendiani, L. Sun, Y. Zhang, T. Li, J. Kim, C. Y. Chim, G. Galli, and F. Wang, Nano Lett. **10**, 1271 (2010).

[15] S. Tongay, J. Zhou, C. Ataca, K. Lo, T. S. Matthews, J. Li, J. C. Grossman, and J. Wu, Nano Lett. **12**, 5576 (2012).
[16] B. Radisavljevic, A. Radenovic, J. Brivio, V. Giacometti, and A. Kis, Nat. Nanotechnol. **6**, 147 (2011).
[17] S.-W. Min, H. S. Lee, H. J. Choi, M. K. Park, T. Nam, H. Kim, S. Ryu, and S. Im, Nanoscale **5**, 548 (2013).
[18] J. Na, M.-K. Joo, M. Shin, J. Huh, J.-S. Kim, M. Piao, J.-E. Jin, H.-K. Jang, H. J. Choi, J. H. Shim *et al.*, Nanoscale **6**, 433 (2014).
[19] C. Rice, R. J. Young, R. Zan, U. Bangert, D. Wolverson, T. Georgiou, R. Jalil, and K. S. Novoselov, Phys. Rev. B **87**, 081307(R) (2013).
[20] S. Horzum, H. Sahin, S. Cahangirov, P. Cudazzo, A. Rubio, T. Serin, and F. M. Peeters, Phys. Rev. B **87**, 125415 (2013).
[21] C. H. Chang, X. Fan, S. H. Lin, and J. L. Kuo, Phys. Rev. B **88**, 195420 (2013).
[22] Y. Cai, J. Lan, G. Zhang, and Y. W. Zhang, Phys. Rev. B **89**, 035438 (2014).
[23] E. Scalise, M. Houssa, G. Pourtois, V. Afanasév, and A. Stesmans, Nano Res. **5**, 43 (2012).
[24] N. Lu, H. Guo, L. Li, J. Dai, L. Wang, W.-N. Mei, X. Wu, and X. C. Zeng, Nanoscale **6**, 2879 (2014).
[25] C. Ataca, M. Topsakal, E. Aktürk, and S. Ciraci, J. Phys. Chem. C **115**, 16354 (2011).
[26] A. Molina-Sánchez and L. Wirtz, Phys. Rev. B **84**, 155413 (2011).
[27] C. Sevik, Phys. Rev. B **89**, 035422 (2014).
[28] D. Çakr, F. M. Peeters, and C. Sevik, Appl. Phys. Lett. **104**, 203110 (2014).
[29] S. Baroni, S. de Gironcoli, A. Dal Corso, and P. Giannozzi, Rev. Mod. Phys. **73**, 515 (2001).
[30] P. Giannozzi, S. Baroni, N. Bonini, M. Calandra, R. Car, C. Cavazzoni, D. Ceresoli, G. L. Chiarotti, M. Cococcioni, I. Dabo *et al.*, J. Phys.: Condens. Matter **21**, 395502 (2009).
[31] D. Vanderbilt, Phys. Rev. B **41**, 7892 (1990).
[32] J. P. Perdew, J. A. Chevary, S. H. Vosko, K. A. Jackson, M. R. Pederson, D. J. Singh, and C. Fiolhais, Phys. Rev. B **46**, 6671 (1992).
[33] L. F. Huang and Z. Zeng, J. Appl. Phys. **113**, 083524 (2013).
[34] A. van de Walle and G. Ceder, Rev. Mod. Phys. **74**, 11 (2002).
[35] N. Mounet and N. Marzari, Phys. Rev. B **71**, 205214 (2005).
[36] D. Yoon, Y. W. Son, and H. Cheong, Nano Lett. **11**, 3227 (2011).
[37] W. Bao, F. Miao, Z. Chen, H. Zhang, W. Jang, C. Dames, and C. N. Lau, Nat. Nanotechnol. **4**, 562 (2009).
[38] W. Pan, J. Xiao, J. Zhu, C. Yu, G. Zhang, Z. Ni, K. Watanabe, T. Taniguchi, Y. Shi, and X. Wang, Sci. Rep. **2**, 893 (2012).
[39] N. D. Mermin, Phys. Rev. **176**, 250 (1968).
[40] J. C. Meyer, A. K. Geim, M. I. Katsnelson, K. S. Novoselov, T. J. Booth, and S. Roth, Nature (London) **446**, 60 (2007).
[41] A. Fasolino, J. H. Los, and M. I. Katsnelson, Nat. Mater. **6**, 858 (2007).
[42] M. Neek-Amal and F. M. Peeters, Phys. Rev. B **83**, 235437 (2011).
[43] J. Brivio, D. T. L. Alexander, and A. Kis, Nano Lett. **11**, 5148 (2011).
[44] T. J. Wieting and J. L. Verble, Phys. Rev. B **3**, 4286 (1971).
[45] S. Najmaei, M. Ajayan, and J. Lou, Nanoscale **5**, 9758 (2013).
[46] S. Sahoo, A. P. S. Gaur, M. Ahmadi, M. J. F. Guinel, and R. S. Katiyar, J. Phys. Chem. C **117**, 9042 (2013).
[47] N. A. Lanzillo, A. G. Birdwell, M. Amani, F. J. Growne, P. B. Shah, S. Najmaei, Z. Liu, P. M. Ajayan, J. Lou, M. Dubey *et al.*, Appl. Phys. Lett. **103**, 093102 (2013).
[48] R. Yan, J. R. Simpson, S. Bertolazzi, J. Brivio, M. Watson, X. Wu, A. Kis, T. Luo, A. R. H. Walker, and H. G. Xing, ACS Nano **8**, 986 (2014).
[49] J. H. Fan, P. Gao, A. M. Zhang, B. R. Zhu, H. L. Zeng, X. D. Cui, R. He, and Q. M. Zhang, J. Appl. Phys. **115**, 053527 (2014).
[50] X. Lu, M. I. B. Utama, J. Zhang, Y. Zhao, and Q. Xiong, Nanoscale **5**, 8904 (2013).
[51] L. F. Huang, T. F. Cao, P. L. Gong, and Z. Zeng, Solid State Commun. **190**, 5 (2014).
[52] B. Fultz, Prog. Mater. Sci. **55**, 247 (2010).
[53] S. H. El-Mahalawy and B. L. Evans, J. Appl. Crystallogr. **9**, 403 (1976).
[54] R. Murray and B. L. Evans, J. Appl. Crystallogr. **12**, 312 (1979).
[55] R. Yan, S. Bertolazzi, J. Brivio, T. Fang, A. Konar, A. G. Birdwell, N. V. Nguyen, A. Kis, D. Jena, and H. G. Xing, arXiv:1211.4136.
[56] J. Wilson and A. Yoffe, Adv. Phys. **18**, 193 (1969).
[57] Y. Wang, J. J. Wang, H. Zhang, V. R. Manga, S. L. Shang, L.-Q. Chen, and Z.-K. Liu, J. Phys.: Condens. Matter **22**, 225404 (2010).